Scientia Iranica A (2021) 28(6), 3092–3111

SCIENTIA IRANICA

Sharif University of Technology
Scientia Iranica
Transactions A: Civil Engineering
http://scientiairanica.sharif.edu

Characteristics of the wall-frame interaction in steel plate shear walls with perforated infill plates

H. Darvishi[a] and M. Mofid[b,*]

a. *Department of Civil Engineering, Sharif University of Technology, Tehran, Iran.*
b. *Center of Excellence in Structures and Earthquake Engineering, Department of Civil Engineering, Sharif University of Technology, Tehran, P.O. Box 11155-9313, Iran.*

Received 20 January 2021; received in revised form 16 February 2021; accepted 13 September 2021

KEYWORDS
Steel plate shear wall;
Perforated infill panel;
Wall-frame interaction;
Ductility ratio;
Perforated ratio;
System strength;
Seismic energy dissipation;
Hysteretic behavior;
Finite element model.

Abstract. The non-linear responses of Steel Plate Shear Walls (SPSWs) with perforated infill plates are studied here with emphasis on the interaction effect between the frame and the infill plate. A number of single- and 14-story SPSWs with solid and perforated infill panels at different perforation ratios are studied numerically. The results are utilized to (a) discuss the influence of perforated ratio and placement of the holes on system behavior, (b) study changes in system strength, stiffness, damping ratio, and ductility due to the introduction of perforation in infill panels, and (c) evaluate the change in behavior of low- and high-rise structures by the introduction of perforations. The results reveal that the perforation ratio is not the only controlling factor in strength and ductility of the shear wall specimens, and the strength and ductility of SPSW also depend upon the placement array of the perforations. The ultimate strength, ductility ratio, and initial stiffness of the perforated SPSWs have been reduced to 28, 29, and 33.5% compared to the reference specimen, respectively. Also, the values of normalized Cumulative Hysteresis Energy (CHE) and Last cycle Hysteresis Energy (LHE) and equivalent viscous damping ratio in perforated specimens are reduced to about 28, 26, and 10%, respectively.

1. Introduction

Utilization of Steel Plate Shear Walls (SPSWs) as a lateral force-resisting system to resist lateral loads such as earthquake and wind forces has grown globally in recent decades [1]. A conventional SPSW is a single or multistory lateral force-resisting system that consists of thin stiffened or unstiffened infill plates surrounded by Horizontal and Vertical Boundary Elements (HBEs and VBEs).

Numerous experimental and analytical research programs have shown that this structural system provides an effective solution for both new construction and retrofitting of existing structures. Furthermore, this system has emerged as an efficient and economically viable alternative to many other lateral load-resisting systems, such as concentric/eccentric braced frames, reinforced concrete shear walls because of advantages like performance, ease of design, foundation cost, fast pace and simplicity of construction, high initial stiffness, substantial ductility, usable space in a building, and reduction of seismic mass [2–13].

Early designs of SPSWs used to have thick or stiffened plates to prevent buckling due to shear stresses forming at low levels of loading, but in recent years, SPSW designs were based on the idea of utilizing the post-buckling capacity.

In a typical SPSW with highly slender infill

*. *Corresponding author. Tel.: +98 21 66164201*
E-mail addresses: h_darvishi65@yahoo.com (H. Darvishi); mofid@sharif.edu (M. Mofid)

doi: 10.24200/sci.2021.57582.5310

plates, buckling occurs at very early stages of loading, precipitating the development of a tension field action that resists the applied lateral forces [1,3]. In other words, the behavior of thin unstiffened SPSWs relies on the development of fold lines of tension field.

To date, a limited scope of literature has been dedicated to the characteristics of the wall-frame interaction in SPSWs with perforated infill plates. Roberts and Sabouri-Ghomi [14] conducted a series of quasi-static cyclic loading tests on unstiffened steel plate shear panels with centrally placed circular openings. They proposed that the strength and stiffness of a perforated panel could be conservatively approximated by applying a linear reduction factor to the strength and stiffness of a similar solid, unperforated panel. Sabouri-Ghomi and Mamazizi [15] experimentally studied the effect of two rectangular openings on the behavior of an SPSW. Alavi and Nateghi [16] carried out an experimental study on several SPSWs that were perforated in the middle of the infill plate in combination with diagonal stiffeners. Pellegrino et al. [17] explored the effect of using a hole with a different size, position, and shape on the nonlinear behavior of infill plates. Berman and Bruneau [18] investigated the use of light-gauge, cold-rolled and Low-Yield Strength (LYS) steel for the infill panel to decrease the strength and stiffness of the panel. In addition, Vian et al. [19] worked on the placement of a pattern of perforations as an effective way to reduce the strength and stiffness of the infill panel. Vian et al. [19,20] investigated the use of Reduced Beam Sections (RBSs) at the ends of the horizontal boundary members as a means to reduce the overall load demand on the vertical boundary members. Purba [21] proposed an equation to determine the shear strength of a perforated infill plate with the specific perforation pattern proposed by Vian et al. [19].

Habashi and Alinia [3] performed a series of finite element analyses to investigate the effects of some important geometrical parameters on the behavior of the SPSWs. The most important investigated parameters included plate thickness, frame height-to-width ratio, and degree of stiffness of unperforated infill panels. Emami and Mofid [22] investigated the practical application of an added Energy Absorbent Element (EAE), subjoined to the SPSW, in order to improve the seismic behavior of the SPSW. A series of parametric studies are implemented to examine the effect of dimensions, position, and formation of the EAE. Akbari Hamed and Mofid [23] employed linear static analyses to investigate the effects of size and location of the shear panel on the lateral stiffness of the frame with respect to the moment-resisting frame with the same member sections. Paik [24] studied the ultimate strength of perforated steel plates under shear loads. Valizadeh et al. [25] designed a typical single-story single-bay SPSW with a solid infill plate to compare its behavior with specimens implementing a circular opening at the center of its infill plate. They demonstrated that the introduction of openings reduced the initial stiffness as well as strength of the system. They also found that the creation of openings significantly decreased the energy absorption capacity of the system. Bhowmick et al. [26] conducted a series of frequency analyses using finite element method to investigate the effects of perforations on periods of SPSWs. Moghimi and Driver [27] studied the demands on the columns of SPSWs with perforated infill plates. Barkhordari et al. [28] investigated the behavior of single- and multi-story SPSWs with stiffened full-height rectangular openings. Afshari and Gholhaki [29] studied the shear strength of single-story one-bay SPSWs with openings at different points of the infill plate using the Finite Element Models (FEMs). The findings of Sabouri-Ghomi et al. [30] illustrated that changing the location of the stiffened opening with the same dimensions had no significant effect on the behavior of SPSW. However, the changes in the location and dimensions of the opening without stiffeners can affect the shear loading capacity of SPSW. Bahrebar et al. [31] investigated the cyclic behavior and energy absorption capacity of SPSWs with trapezoidal corrugated infill plates that were centrally perforated. Deylami and Daftari [32] investigated the effect of varying geometrical parameters on the behavior of SPSWs with rectangular openings at the center of the infill plate by modeling over 50 FEMs. They concluded that the introduction of openings even at low percentages resulted in severe loss of shear capacity of the SPSW. Farzampour et al. [33] conducted a numerical study on SPSW models with flat and corrugated infill plates with openings. Saad-Eldeen et al. [34] experimented a series of high tensile steel stiffened plates with multiple openings to investigate different degrees of openings by various sets of openings. Shekastehband et al. [35] conducted experimental and numerical studies on the seismic behavior of semi-supported steel shear walls. Phillips and Etherton [36] used FEMs to investigate the behavior of experimental specimens and the buckling of ring shaped-steel plate shear walls and developed useful design equations for them. Mu and Yang [37] investigated the influence of frame-to-plate connections and oblique channel-shaped stiffeners on the structural behavior of SPSWs with openings experimentally. Paslar et al. [38] proposed equations for SPSWs with circular openings based on the regression analysis. Khan and Srivastava [39] demonstrated that the size and location of the openings could have significant effects on the performance of SPSWs.

Yekrangnia and Asteris [40] proposed a multi-strut macro-model, capable of simulating the overall force-displacement behavior of infilled frames with various opening configurations. They showed that the

size of the opening along with its position, compared to the size of the infill wall, could significantly affect both the inclination and the effective width of the struts and the overall behavior of infilled frames with openings. Asteris et al. [41] provided a thorough overview of the different micromodels proposed for the analysis of infilled frames. They pointed to the advantages and disadvantages of each micromodel and presented practical recommendations for the implementation of the different models. Cavaleri et al. [42] investigated the nonlinear behavior of infills and the arch effect between unreinforced masonry infills and the surrounding frames. Lemonis et al. [43] presented an analytical model to estimate the initial lateral stiffness of steel moment-resisting frames with masonry infills.

Based on the literature review and the author's knowledge, there is almost no specific work that explains the characteristics of wall-frame interaction of perforated SPSWs with different aspect ratios, especially in multi-story high-rise buildings. In this study, the interaction of the frame and the infill plate in SPSW in high-rise specimens as well as single-story specimens has been investigated and the effect of the presence of holes on the behavior of the samples has been studied. Also, most studies on perforated SPSWs have focused on the effect of the presence of holes or openings on the ultimate strength capacity of the specimen. Most of these studies concentrate on relating the yield strength of perforated infill plates with a linear reduction factor to the yield strength of solid infill plates [14,20,30,44]. Most of the relationships presented by the researchers are proportional to the perforation ratio of the infill plate. However, as shown in Figure 1, a perforated SPSW with the same perforation ratio can have different arrangements of holes. Since the main source of energy absorption in an SPSW is the infill plate deformation as an energy-absorbing member, the amount of available material and the arrangement of the holes can have a significant effect on the important structural parameters, especially the amount of energy absorption and damping coefficients. It is known that SPSWs regarding the frame and infill plate actions are treated like a dual system. In this regard, frame and infill plates are treated like two subsystems. Thus, a good estimate of the role of each subsystem in resisting lateral loads can help establish a design procedure as well as controlling damages to frame members. It can reduce rehabilitation costs after a severe or moderate earthquake. Because of the complex behavior of perforated SPSWs due to the post-buckling strength of the infill panel, establishing an explicit interaction between infill plates and boundary members in a close-form solution seems to be very difficult. However, the use of FEM can help establish a good relationship between the frame and infill plates subsystems.

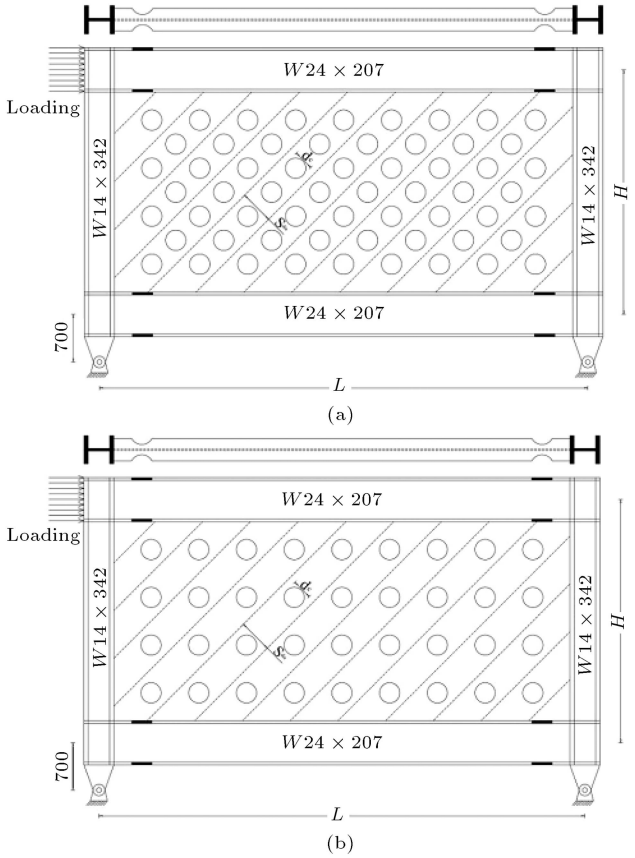

Figure 1. (a) Perforated Steel Plate Shear Wall (SPSW) with type-I infill panel. (b) Perforated SPSW with type-II infill panel.

In this study, a number of SPSW models with solid and perforated infill plates is numerically analyzed using FEM and the results are employed to discuss (a) the effect of using perforated infill panels instead of solid infill panels on frames' behavior, (b) the influence of perforated ratio and placement of the holes on system behavior, (c) changes in system strength, stiffness, damping ratio, and ductility due to the introduction of perforation in infill panels, and (d) evaluate the change in behavior of low- and high-rise structures by the introduction of perforations.

2. Method of study

2.1. Models description

In this research, a number of 1- and 14-story SPSWs with different aspect ratios and solid and perforated infill plates are designed and studied. One- and fourteen-story buildings with a fixed story height of 3.6 m are considered. It is assumed that the beam-to-column connections of the boundary frame are pinned and they do not participate in design and analysis. Also, the gravitational loads are not tolerated by the steel shear wall beams and are transmitted by the transverse beams to the beam-to-column connections.

Table 1. Geometric characteristics of Steel Plate Shear Wall (SPSW) specimens.

Name	Number of stories	Bay width (m)	Number of steel plate shear walls in each loading direction
1S1	1	3.6	2
1S1.5	1	5.4	2
1S2	1	7.2	2
1S2.5	1	9	4
1S3	1	10.8	4
14S1	14	3.6	6
14S2	14	7.2	6
14S3	14	10.8	4

Table 2. Steel Plate Shear Wall (SPSW) element dimensions: 1-story SPSWs with solid infill.

Specimens	Plate thickness (mm)	HBE[a] size	VBE[b] size
1S1	3.2	$W18 \times 106$	$W14 \times 233$
1S1.5	3.2	$W21 \times 132$	$W14 \times 257$
1S2	3.2	$W24 \times 207$	$W14 \times 342$
1S2.5	3.2	$W24 \times 229$	$W14 \times 500$
1S3	3.2	$W24 \times 306$	$W14 \times 665$

Note: [a]HBE: Horizontal Boundary Element; [b]VBE: Vertical Boundary Element.

Table 3. Steel Plate Shear Wall (SPSW) element dimensions: 14-story SPSWs with solid infill.

Story	14S1			14S2			14S3		
	Plate thickness (mm)	HBE[a] size	VBE[b] size	Plate thickness (mm)	HBE size	VBE size	Plate thickness (mm)	HBE size	VBE size
1	6.4	$W14 \times 90$	$W36 \times 800$	4.8	$W14 \times 74$	$W36 \times 800$	6.4	$W16 \times 100$	$W36 \times 800$
2	6.4	$W14 \times 90$	$W36 \times 800$	4.8	$W14 \times 74$	$W36 \times 800$	6.4	$W16 \times 100$	$W36 \times 800$
3	6.4	$W14 \times 90$	$W36 \times 800$	4.8	$W14 \times 74$	$W36 \times 800$	6.4	$W16 \times 100$	$W36 \times 800$
4	6.4	$W14 \times 90$	$W36 \times 800$	4.8	$W14 \times 74$	$W36 \times 800$	6.4	$W16 \times 100$	$W36 \times 800$
5	6.4	$W14 \times 90$	$W36 \times 800$	4.8	$W14 \times 74$	$W36 \times 800$	6.4	$W30 \times 261$	$W36 \times 800$
6	6.4	$W14 \times 90$	$W36 \times 800$	4.8	$W14 \times 74$	$W36 \times 800$	4.8	$W16 \times 100$	$W36 \times 800$
7	6.4	$W24 \times 176$	$W36 \times 800$	4.8	$W14 \times 74$	$W36 \times 800$	4.8	$W16 \times 100$	$W36 \times 800$
8	4.8	$W14 \times 90$	$W36 \times 800$	4.8	$W24 \times 207$	$W36 \times 800$	4.8	$W16 \times 100$	$W36 \times 800$
9	4.8	$W14 \times 90$	$W36 \times 652$	3.2	$W12 \times 53$	$W36 \times 652$	4.8	$W30 \times 261$	$W36 \times 800$
10	4.8	$W24 \times 176$	$W36 \times 652$	3.2	$W12 \times 53$	$W36 \times 652$	3.2	$W14 \times 61$	$W36 \times 652$
11	3.2	$W12 \times 50$	$W36 \times 361$	3.2	$W12 \times 53$	$W36 \times 361$	3.2	$W14 \times 61$	$W36 \times 652$
12	3.2	$W12 \times 50$	$W36 \times 361$	3.2	$W12 \times 53$	$W36 \times 361$	3.2	$W14 \times 61$	$W36 \times 652$
13	3.2	$W12 \times 50$	$W36 \times 361$	3.2	$W12 \times 53$	$W36 \times 361$	3.2	$W14 \times 61$	$W36 \times 529$
14	3.2	$W21 \times 122$	$W36 \times 361$	3.2	$W24 \times 207$	$W36 \times 361$	3.2	$W27 \times 235$	$W36 \times 529$

Note: [a]HBE: Horizontal Boundary Element; [b]VBE: Vertical Boundary Element.

The SPSWs with a solid infill plate are designed according to the recommendations provided by AISC-341, AISC-360, and AISC Design Guide 20. In the case of SPSWs with a perforated infill plate, the dimensions of all components have been considered like SPSWs with a solid infill plate in order to be able to compare the results with the reference model (SPSWs with solid infill plate). Table 1 describes the general characteristics of conventional SPSWs with a perforated infill plate used in the buildings. Also, the specifications of the boundary members of the frame and infill plate for different specimens with 1 and 14 stories are presented in detail in Tables 2 and 3, respectively. The SPSWs with a solid infill plate, which serve as the reference specimens, are designed using the Plate-Frame Interaction (PFI) theory [14,45–48]. The

PFI model has the ability to predict the behavior of SPSWs with different infill plates in the presence and absence of openings, holes, or stiffeners. This model provides a simple tool for designers to effectively design different types of SPSWs with different configurations by considering the behavior of the frame and the infill plate separately. This method considers the behavior of the infill plate and the boundary frame separately and predicts the overall behavior of the system by considering the interaction of these components with each other. In this way, the shear force of each infill plate and the boundary frame is obtained separately. Then, by superimposing the effect of the two subsystems, the shear force of the frame-infill plate dual system of SPSW is obtained.

Two types of regular patterns of perforations of infill panels are investigated. The schematic typical infill panel configuration that has been used in this study is shown in Figure 1. SPSWs are categorized into two major Type I (Figure 1(a)) and Type II (Figure 1(b)). A regular pattern of perforations with diameter d_c is formed at 707 mm from the center to the center of each other. To carry out a parametric study, d_c/S_{diag} as perforation ratio is used. S_{diag} is the width of imaginary diagonal strips that was introduced first by Vian et al. [19], as shown in Figure 1(a) and (b). These parameters are the same for the other specimens with different perforation ratios. The general name of one story perforated specimens is [(number 1) P (number 2) S (number 3)]. Number 1 shows the type of perforation. Digit 1 presents Type I and digit 2 presents Type II of perforation. Number 2 shows the aspect ratio (L/H) of the specimen, and number 3 introduces the perforation ratio (d_c/S_{diag}) of the infill panel. Also, the general name of SPSWs with a solid infill plate is [(number 1) S (number 2)]. Number 1 shows the number of stories. Number 2 shows the aspect ratio (L/H) of the specimen.

To design all specimens, the minimum applicable thickness for welding which is 3.2 mm is considered. The general height of the specimens is such that the center-to-center distance between the upper and lower beams is $H = 3.6$ m. The length of beams is selected in such a way that the aspect ratios ranged from 1 to 3 (i.e., L/H=1, 1.5, 2, 2.5, and 3); and the ratio of perforation ranging from 0.2 to 0.6 is selected for investigation. The web thickness of stiffener plates in columns is similar to that of the beam flanges.

To withstand the ever greater loads resulting from tension field and reach the optimum design, the beams are designed as RBS. RBS connections are applied to the design of special moment frames whose details are presented by FEMA 350 (FEMA 2000) [49] and AISC 358–05 [50].

The beam-column connection details include RBS at each end to ensure inelastic beam action at the desired locations. By utilizing RBS, the safety of the beam-column connection is taken into account.

2.2. Material properties

ASTM-A572 and ASTM-A36 conventional structural steel standards are selected for frame members and infill panels, respectively. For all incremental pushover and cyclic analyses, the "hardening = combined" model of SUT-DAM [51] was used to represent the stress-strain behavior of the infill plate material (A36) as well as the frame member material (A572). This material model implements the concepts of both isotropic and kinematic hardening.

The kinematic hardening component of the material could be defined in several ways. Since only standard monotonic uniaxial test results for specimen material coupons (i.e., both panel and boundary elements) are available, several assumptions are required to determine the mechanical material properties of the analytical model. In order to study the nonlinear behaviors of infill panels and frame members, the respective stress-strain diagrams that define the constitutive behavior of the two steel materials with $E = 200$ GP and $\nu = 0.3$, as depicted in Figure 2, are selected and used in the FEMs. The yield strengths of the infill panel and frame members are selected as 330 and 385 MPa, respectively.

2.3. Numerical finite element modeling

This study adopts a finite element approach with an implicit integration algorithm. All Eigen-value,

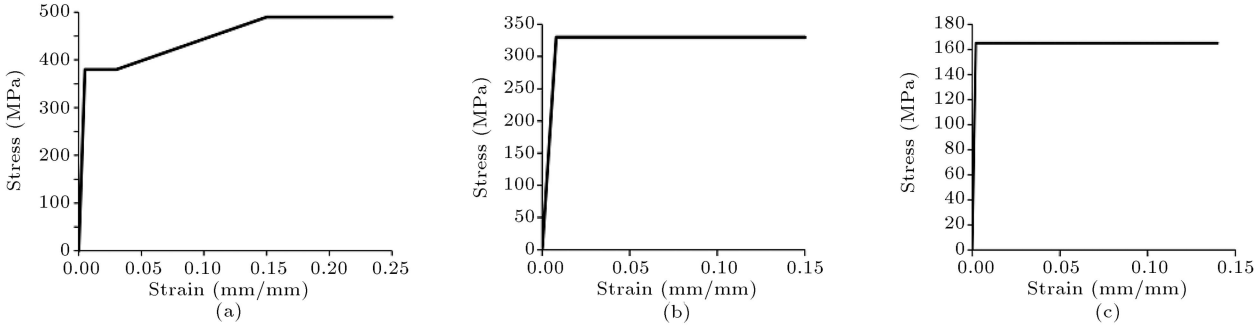

Figure 2. Material properties: (a) Frame members, (b) infill panel (A36), and (c) infill panel (LYS).

incremental nonlinear pushover, and cyclic analysis are carried out using SUT-DAM finite element package [51]. All boundary elements (i.e., HBEs and VBEs) and infill panel elements are modeled by an 8-node, quadrilateral, stress displacement shell element with reduced integration (to achieve more accurate results and significantly reduce computing and running times) and large strain formulations (to capture the out-of-plane behavior of infill plates).

2.4. Boundary conditions

To refrain from the lateral torsion buckling phenomenon, the top flange of the top beam was restrained from out-of-plane displacement. Furthermore, the out-of-plane displacements of the beam webs restrained to simulate the constraints are imposed by slab of the story floors. All degrees of freedom, except the rotation about the out-of-plane axis, are restrained to allow the formation of plastic hinges only in RBS connection (in the bottom beam as well as top beam). Thus, the stiffness of the dual system of frame and infill plate is the main factor that resists the rotation of the frame.

To consider the initial imperfections (the out-of-plane deformations) produced due to the construction errors (which cause the plate not to be completely flat), a buckling analysis was first performed to obtain the eigenvalue vectors. The first buckling mode was multiplied by the magnitude of a small displacement (1 mm) and applied to all specimens as the initial boundary conditions.

Displacement corresponding to a 20% drop in the maximum shear capacity of the sample is considered as the ultimate displacement (δ_u) by FEMA-P695 and FEMA-356. This criterion represents the material damage by considering the overall system stability under $P-\Delta$ effects. On the other hand, according to the laboratory studies in all specimens, major structural damage in drift displacements of more than 3% occurs in the connections. Also, the maximum displacement value corresponding to 2.5% drift is considered as the ultimate displacement (δ_u) by ASCE-07. Therefore, the displacement value corresponding to the minimum value provided by these three criteria was considered as the ultimate displacement of the specimens. For all specimens, the ultimate displacement value (δ_u) was considered equal to 90 mm (2.5% drift).

2.5. Validation and verification of results

The validation and authenticity of the finite element modeling, boundary conditions, simulation of mechanical behavior of the materials, and loading procedures were verified by comparing published test results provided by Choi and Park [52] and Vian et al. [19] with the corresponding analysis results obtained from SUT-DAM FEMs. According to the loading history used in the laboratory models, in-plan cycle loading was applied on both sides of the upper beam.

A comparison between the hysteresis cycles obtained from both the one-story (Figure 3) and three-story models (Figure 4) clearly demonstrates the alikeness between the results of the experiments and FEMs. The contours of Von-Mises stress distribution of the FEMs corresponding to the considered experiment specimens are shown in Figures 3 and 4, respectively.

Figure 5 depicts the typical diagrams of "lateral load-displacement" and "stiffness-drift ratio" for a conventional shear wall with solid and perforated infill plates ($D/S = 0.4$).

3. Discussion of results

3.1. General behavior

Based on the research presented by Habashi and Alinia [3] and Hosseinzadeh and Tehranizadeh [6], the general behavior of SPSWs is divided into three stages. Likewise, the general behavior of an SPSW with solid infill plates is described and compared with an SPSW with a perforated infill plate by dividing the diagrams into three regions.

OA: In the case of extremely small lateral loads, both systems of an SPSW with a perforated infill plate and a typical solid infill plate exhibit elastic behavior. At the center of the infill plates and far from the boundary members, the plates are exposed to a net shear with principal tension and compression stresses which are equal and located in 45 degrees to the loading direction. With increasing load, since the infill plates in both systems are extremely thin, buckling occurs in them due to principal compression stresses. Hence, the infill plate becomes geometrically non-linear and both systems lose a substantial portion of their stiffness. Nonetheless, SPSWs with larger perforation ratios experience greater stiffness reduction, while SPSWs with smaller perforation ratios experience less stiffness reduction.

When the buckling occurs, the resistance mechanism against the lateral load varies from the in-plane shear of the plate to the inclined tension field. Also, plate deformation continues after buckling until the first yield point occurs in the infill panels (point A in Figure 5). At this level, the difference between the push-over diagrams of the two systems is negligible. However, the reduction in system stiffness is much greater in the specimen with a higher perforated ratio. Identically, in all SPSWs with different perforation ratios, the boundary frame is essentially elastic and stress levels are totally negligible. Figure 6 shows the von Mises stress distribution in SPSWs with conventional solid infill plate and perforated infill plate (with perforated ratio equal to 0.4) corresponding to point A

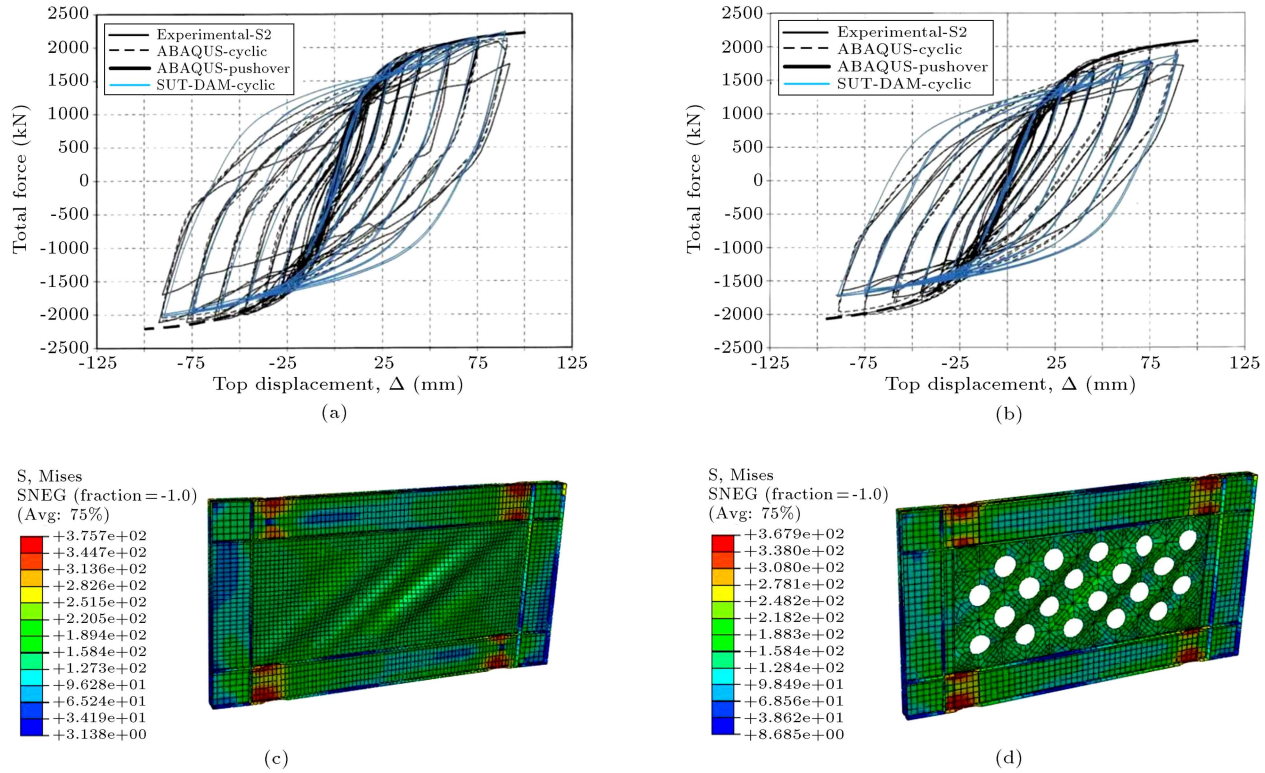

Figure 3. (a) Comparison of the pushover analysis test results of [19] and solid infill plate. (b) Comparison of pushover analysis test results of [19] with perforated infill plate. (c) Von Mises stress distribution of Finite Element Model (FEM) of specimen with solid infill plate in the ultimate state. (d) Von Mises stress distribution of FEM of the specimen with a perforated infill plate in the ultimate state.

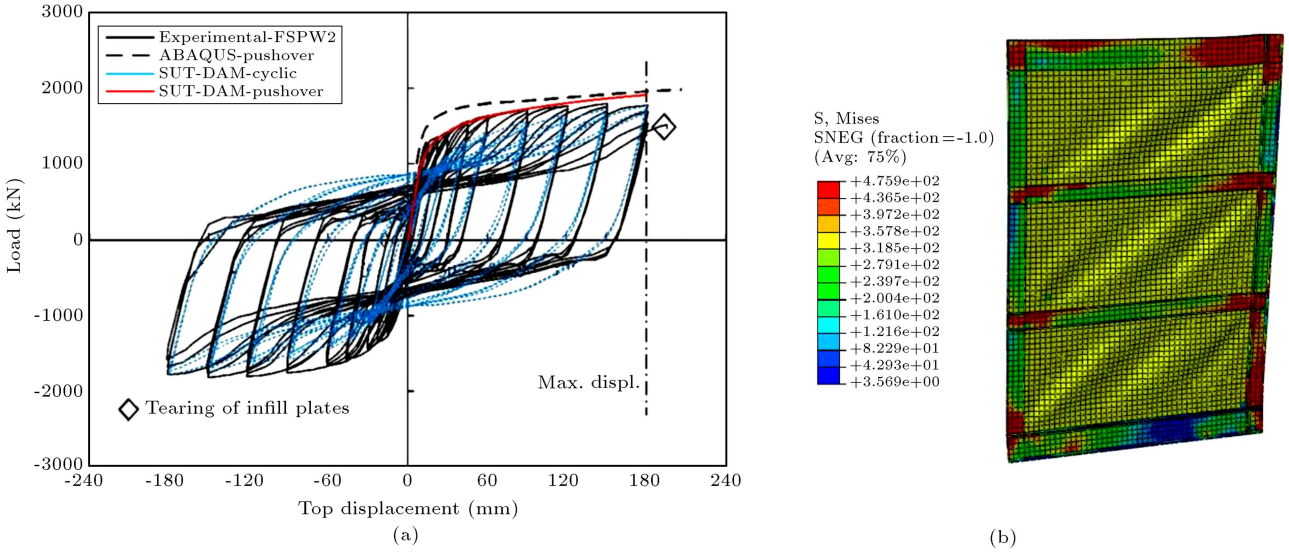

Figure 4. (a) Comparison of pushover analysis with test results of [52]. (b) Von-Mises stress distribution of the corresponding Finite Element Model (FEM) at the ultimate state.

in Figure 5. As seen in Figure 6, the first yield does not necessarily occur on the entire surface of the infill plates, whether solid or perforated.

AC: In the next stage, the infill panels of both systems become non-linear from the material and geometrical viewpoints, while the boundary frames are elastic and yield area expands throughout the infill plates. The stiffness of both systems is almost constant until the formation of yield areas (point B) and it is associated with a sensitivity reduction. However, the stiffness of the SPSW with a solid infill plate is slightly higher

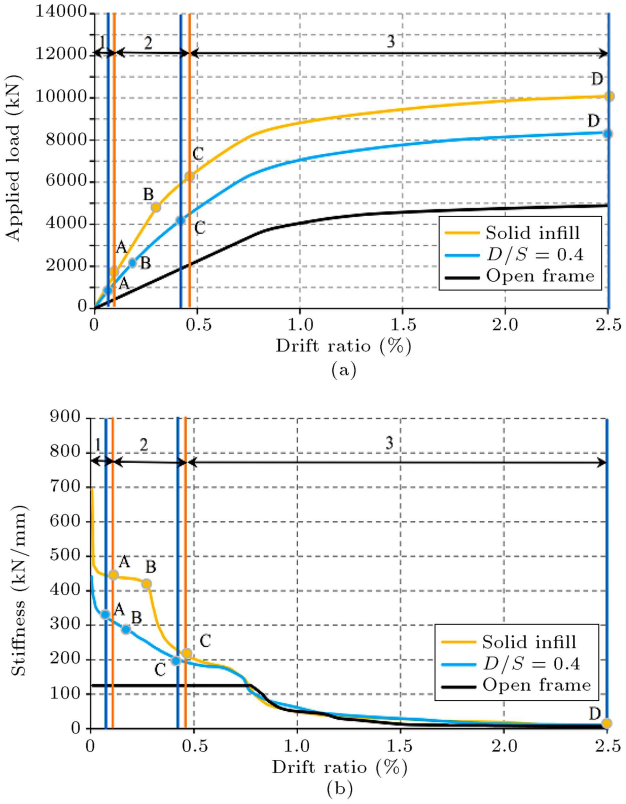

Figure 5. (a) Typical lateral load-displacement curves of Steel Plate Shear Walls (SPSWs) with solid infill and perforated infill panels at a perforation ratio of 0.4. (b) Typical stiffness-displacement curves of (SPSWs) with solid infill and perforated infill panels at a perforation ratio of 0.4.

than that of the specimen with a perforated infill plate until point C which is relative to the first yield point in the frame members. Similarly, both specimens lose significant stiffness due to the considerable yield of the infill panels (except the zone between holes and besides the boundary frames away from the center of the infill panel). At this point, load-displacement diagrams of the specimens began to separate from each other. The difference between the diagrams, however, is not remarkable. Figure 7 shows the von-Mises stress distribution of SPSWs with solid infill plate and perforated infill (with perforated ratio equal to 0.4) corresponding to point C in Figure 5.

CD: During the third stage, in both specimens, frame materials become non-linear and all infill panels completely yield (except the regions between the perforations in perforated specimens). The RBS connection zone is completely turned into a plastic hinge and ultimately both specimens have reached their ultimate capacity at point D. In this stage, the stiffness of both systems is approximately equal. However, the difference between the load-displacement curves of the two specimens slightly increases (up to 16% in this case).

Von-Mises stress distribution of SPSWs with a solid infill panel and a perforated infill panel (with a perforated ratio equal to 0.4) is shown at their ultimate capacity in Figure 8. At this point, the yield area has expanded all across the infill plates and the plastic hinges occurred in the RBS connection.

3.2. Characteristic of the frame-infill plate behavior

Comparison and measurement of the absorbed shear by each component of frame and infill plate is an effective way to assess the behavior of the infill panels in SPSWs with solid and perforated infill plates and different perforation ratios.

The values of absorbed shear forces are calculated by integrating shear stresses across the width of the infill plates. Roles of various infill plates in withstanding the shear forces as a percentage of the whole tolerated shear by the SPSWs with solid and perforated infill plates at different perforation ratios are illustrated in Figures 9 and 10. In other words, the ultimate values of shear forces resisted by the infill plates with different drift ratios are depicted in Figure 9. As shown in Figures 9 and 10, both solid and perforated infill plates of SPSW have similar behavior. However, their ultimate strength is not equal.

As shown in Figures 9 and 10, the infill plates in both specimens with solid and perforated plates reach their ultimate strength at a drift ratio equal to 1%,

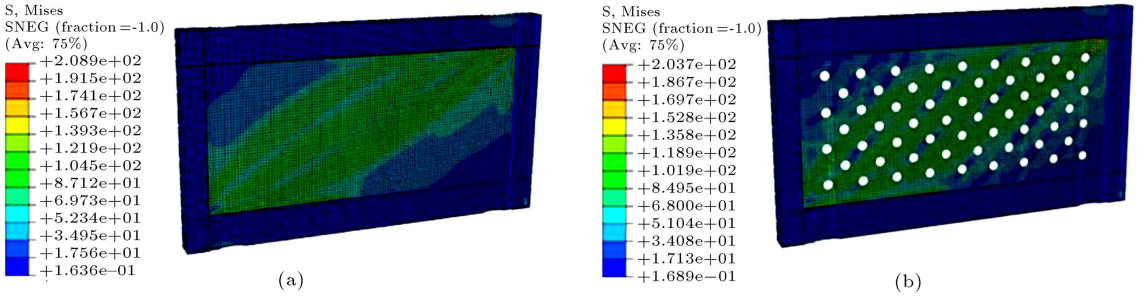

Figure 6. Von-Mises stresses in Steel Plate Shear Walls (SPSWs) with solid and perforated infill panels at point A: (a) S2 specimen and (b) 1P2S04 specimen (with perforated ratio equal to 0.4).

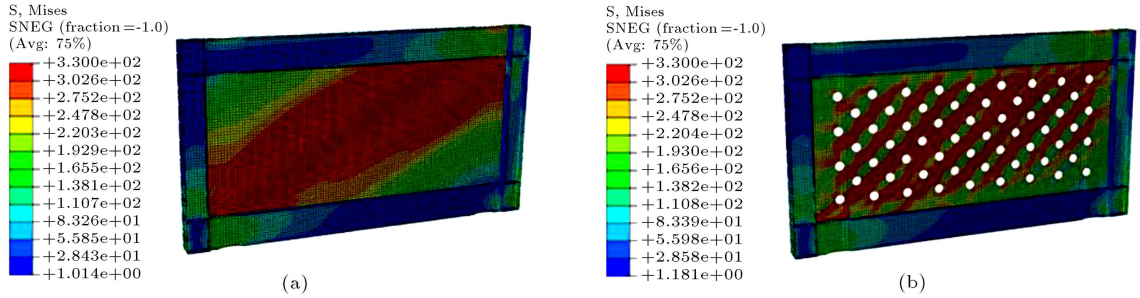

Figure 7. Von-Mises stresses in Steel Plate Shear Walls (SPSWs) with solid and perforated infill panels at point C: (a) S2 specimen and (b) 1P2S04 specimen (with perforated ratio equal to 0.4).

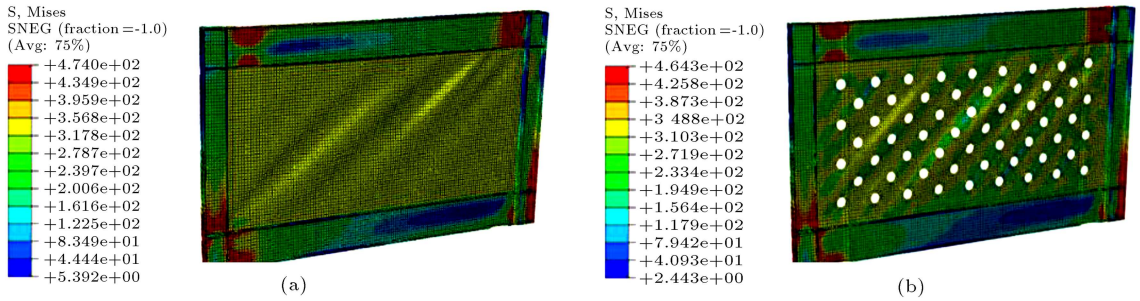

Figure 8. Von-Mises stresses in Steel Plate Shear Walls (SPSWs) with solid and perforated infill panels at point D: (a) S2 specimen, and (b) 1P2S04 specimen (with perforated ratio equal to 0.4).

approximately. Furthermore, Figures 9 and 10 show the infill plate participation in resisting lateral shear forces of an SPSW with solid and perforated infill plates with different perforation and aspect ratios. As observed in Figure 9, the participation percentage for different plates in resisting the shear forces decreased by increasing the perforation ratio (up to 18% reduction in case of $L/H = 3$). The reduction in infill plate participation is greater in bearing shear forces at small drifts. This reduction in participation in resisting the shear forces decreases following an increase in drift ratios and the percentages of participation become convergent.

The comparison between the participation percentage curves demonstrates that the participation percentage of the infill plate in bearing the lateral loads for different specimens before the drift of 0.1% (where the first yield occurs in the infill plate) is approximately equal. Afterward, the curves of participation percentage at different levels begin to converge and become flat and finally horizontal.

3.3. Results of quasi-static cyclic analyses

Quasi-static cyclic analyses were performed on models with two different perforation patterns to investigate the behavior of the specimens and to perform parametric studies. The most important structural parameters studied to compare the results are yield and ultimate strength, yield displacement, initial stiffness, hysteresis energy, and equivalent viscous damping. The effect of the position of the perforations was investigated by studying several series of one-story SPSWs with an aspect ratio of $L/H = 2$ with two different perforation patterns. Figure 11(a) shows the hysteresis behavior of the reference model with a solid infill plate without perforations and the corresponding backbone curve (dashed line). The bilinear curve is fitted according to the method presented in FEMA-356 with the backbone curve according to the dashed line in Figure 11(b). According to this method, to calculate the initial stiffness, 60% of the yield strength of the specimen was used ($K_i = 4.34 \times 10^5$ kN/m). Also, the strain hardening (K_h) equal to 2.56×10^4 kN/m was used to produce a bilinear curve to the maximum loading point up to 10074 kN. As a result of fitting the bilinear lateral load-displacement curve, the effective yield deformation (δ_y) equals 19 mm and the overall yield strength (V_y) equals 6938.8 kN. As a result of fitting the bilinear lateral load-displacement curve, the overall yield strength (V_y) equals 6938.8 kN and the effective yield deformation (δ_y) is equal to 19 mm.

In the initial stages of loading, significant buckling of the infill plate with the less insignificant participation of the boundary frame than the infill plate in resisting lateral loads has led to a significant pinching in the system hysteresis curve. Following the introduction of holes and the consequent reduction of the participation of the filler sheet in bearing lateral loads, even in the initial stages of loading with increasing the bearing share of the boundary frame, the pinching

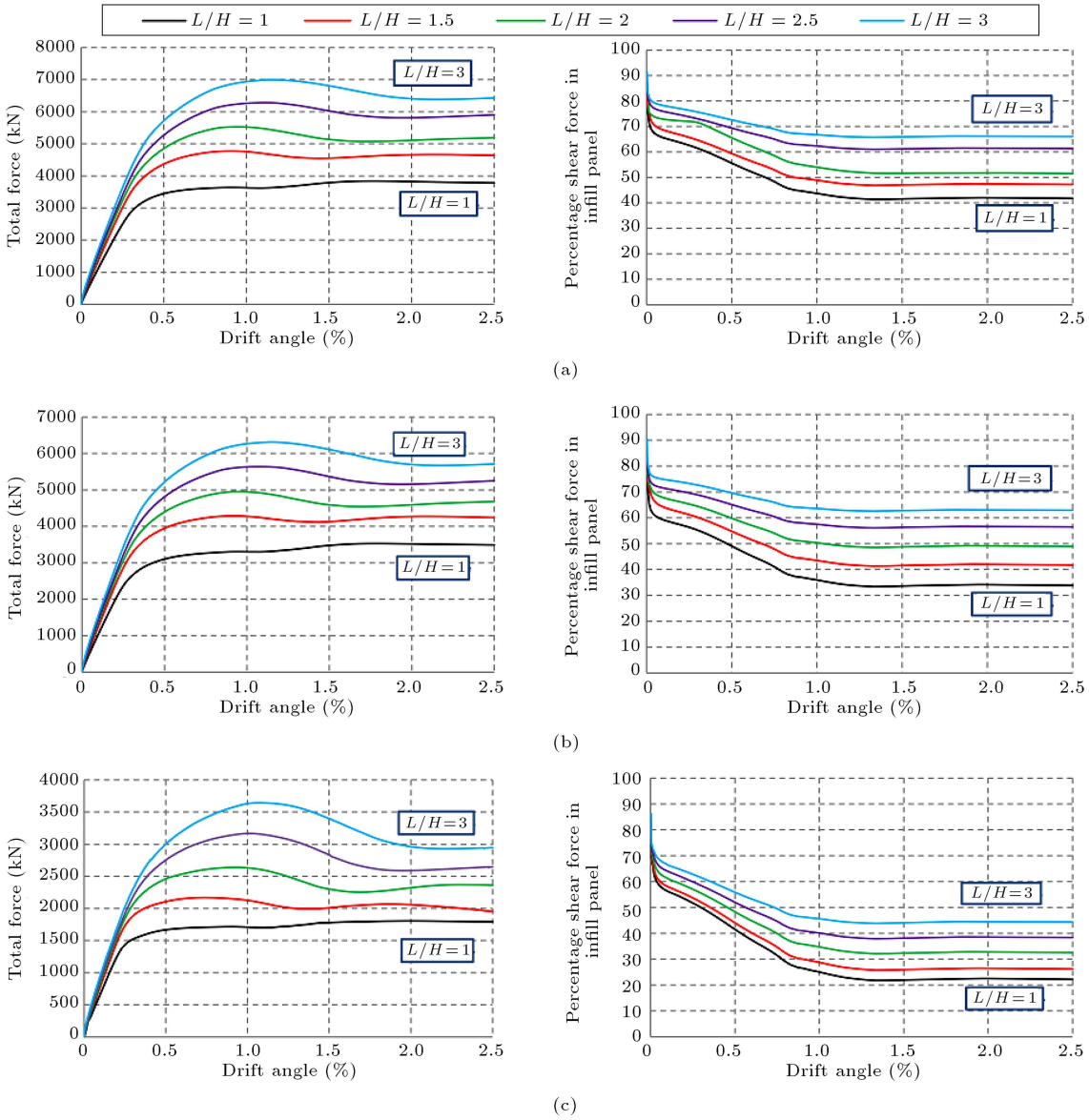

Figure 9. Comparison of the absorbed shear forces by the infill plates with the percentage of shear forces absorbed by the infill plates of Steel Plate Shear Walls (SPSWs) with different aspect ratios: (a) Solid infill, (b) $D/S = 0.2$, and (c) $D/S = 0.6$.

of the hysteresis curve was reduced. By introducing the perforations and subsequently reducing the contribution of the infill plate to resisting the lateral loads, the pinching of the hysteresis curve is reduced. This is evident even in the early stages of loading due to the increased share of the boundary frame in bearing lateral loads. The Cumulative Hysteresis Energy (CHE) and the Last cycle Hysteresis Energy (LHE) for the reference specimen are 8886 and 1133 kJ, respectively. The last cycle is presented in Figure 11 by a dotted line. Since hysteresis energy is a function of shear capacity, it is not correct to simply compare them in different models. Hence, both CHE and LHE have been normalized with the area under the backbone curve. The normalized CHE and LHE of the control specimen are 12.08 and 1.54, respectively. In addition, the equivalent viscous damping ratio (β_{eq}) is calculated based on the data of the last hysteresis cycle by Eq. (1):

$$\beta_{eq} = \frac{LHE}{2\pi V_u \delta_u}, \tag{1}$$

where δ_u and V_u are the ultimate displacement and strength of the last cycle, respectively, and LHE is the area surrounded by the last hysteresis loop. The results of the parametric study of perforated SPSWs with different arrangements of perforations and corresponding SPSW with a solid infill plate are presented in Table 4. The method used to calculate the hysteresis energy, equivalent viscose damping ratio, initial stiffness, and

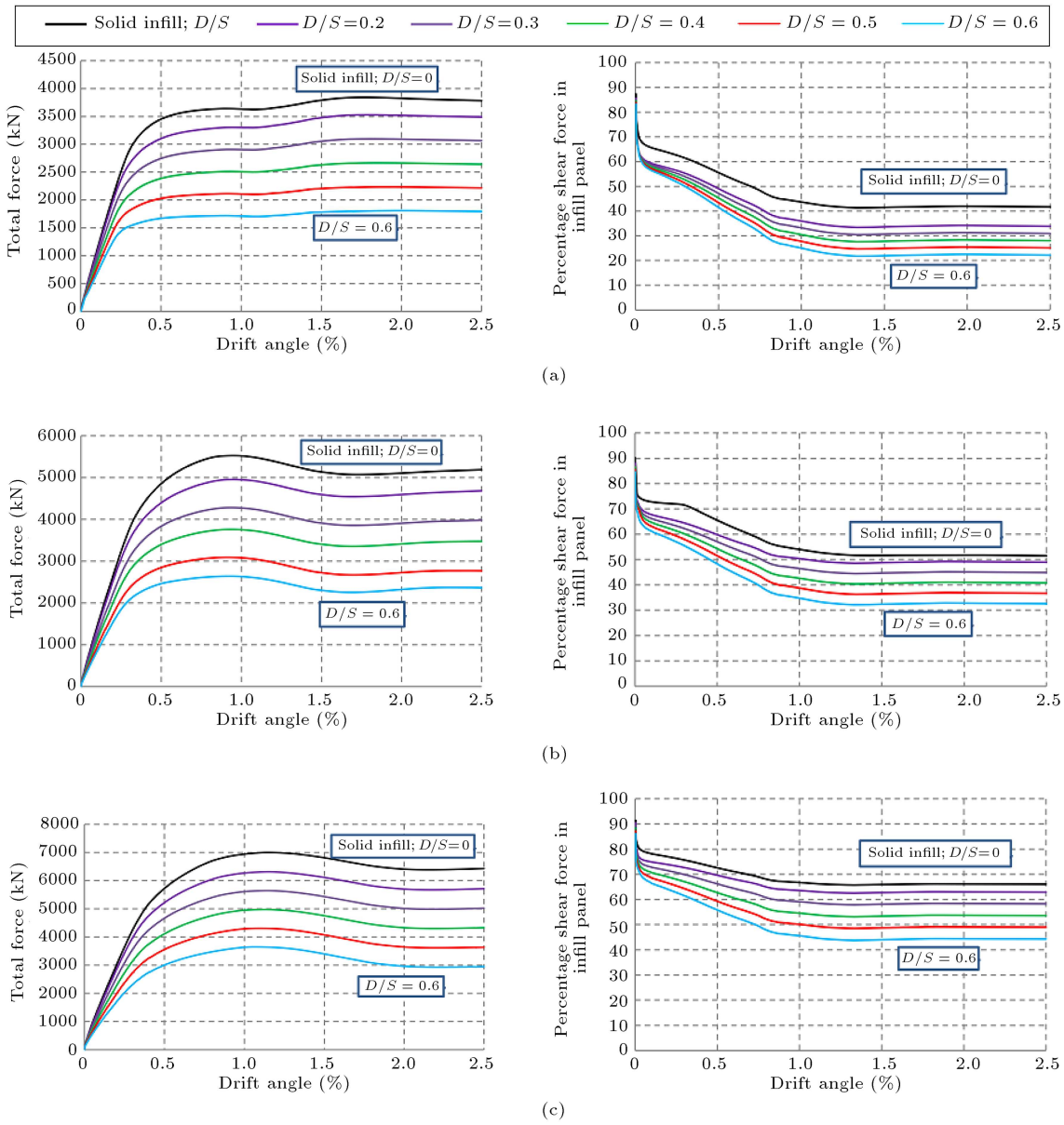

Figure 10. Comparison of the absorbed shear forces by the infill plates and percentage of the shear forces absorbed by the infill plates of Steel Plate Shear Walls (SPSWs) with different perforation ratios: (a) $L/H = 1$, (b) $L/H = 2$, and (c) $L/H = 3$.

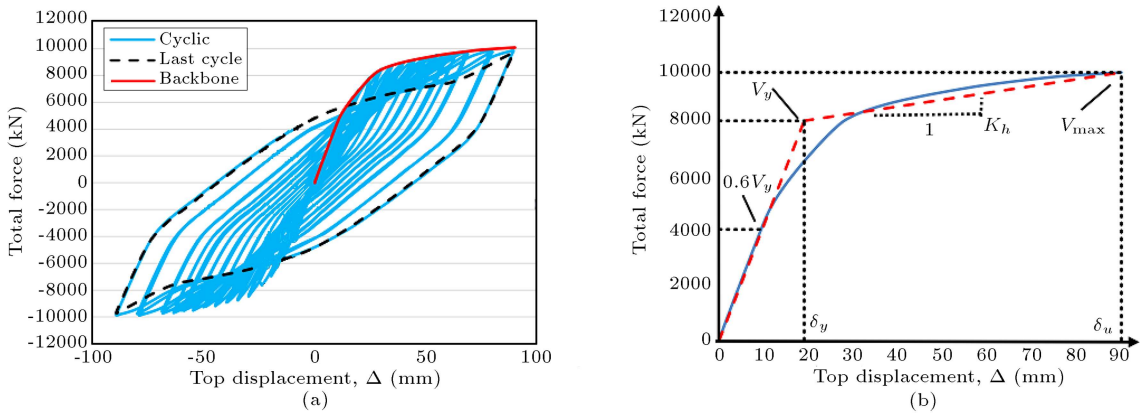

Figure 11. Cyclic results of model 1St.6: (a) Hysteresis behavior and (b) ideal bilinear diagram.

Table 4. Effects of different perforation locations and sizes on the structural parameters of the Steel Plate Shear Walls (SPSWs) specimens.

Model	Initial stiffness (Ki)	V_y	V_u	δ_y	δ_u	Cumulative Hysteresis Energy (CHE)		Last cycle Hysteresis Energy (LHE)		β_{eu}	μ
	kN/m	kN	kN	mm	mm	kJ	Normalized	kJ	Normalized	%	
1S2	4.37E+05	8256.2	10074.54	19.14	90	8886	12.08	1133	1.54	19.90	4.93
1P2S0.2	3.91E+05	7771.78	9570.3	20.08	90	7819.68	11.20	997.04	1.43	18.43	3.46
1P2S0.3	3.74E+05	7595.52	8865.66	22.3	90	7197.46	10.65	917.73	1.36	18.31	3.3
1P2S0.4	3.46E+05	7347.84	8360.48	23.67	90	6753.38	10.32	861.08	1.32	18.22	3.15
1P2S0.5	3.21E+05	6935.04	7656.78	24.71	90	5775.9	9.36	736.45	1.19	17.02	3.07
1P2S0.6	2.91E+05	6687.36	7248.64	25.83	90	5242.74	8.81	688.47	1.12	16.32	3.03
2P2S0.2	4.03E+05	8008.32	9772.32	19.89	90	8263.98	11.59	1053.69	1.48	19.08	3.54
2P2S0.3	3.89E+05	7843.2	9369.36	21.13	90	7730.82	11.07	985.71	1.41	18.61	3.43
2P2S0.4	3.63E+05	7512.96	8764.92	21.79	90	7197.66	10.76	917.73	1.37	18.53	3.32
2P2S0.5	3.35E+05	7347.84	8460.48	22.34	90	6842.22	10.46	872.41	1.33	18.24	3.28
2P2S0.6	3.08E+05	7182.72	8157.52	23.84	90	6486.78	10.14	834.09	1.29	17.94	3.14

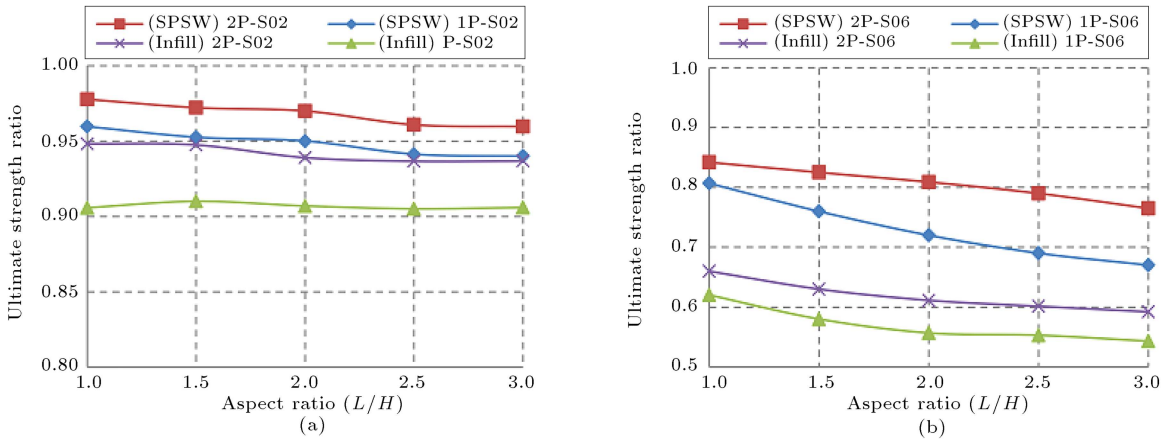

Figure 12. Variations of the ultimate strength ratios of frame, infill plate, and Steel Plate Shear Wall (SPSW) with different aspect ratios and perforated ratios: (a) $D/S = 0.2$ and (b) $D/S = 0.6$.

conversion of the load-displacement curve to the ideal bilinear curve is the same for all specimens.

Comparison of the results shows that the presence of perforations has a significant effect on the ultimate strength, ductility ratio, and initial stiffness of the specimens (the ultimate strength, ductility ratio, and initial stiffness of the perforated SPSWs with the Type-I perforation pattern have been reduced to 28, 29, and 33.5% compared to the reference specimen, respectively). Furthermore, the effect of introducing perforations on normalized CHE and LHE is considerable. In most perforated specimens, the normalized CHE and LHE values and the equivalent viscous damping ratio are significantly reduced compared to the reference specimen with a solid infill plate (normalized CHE and LHE values and the equivalent viscous damping ratio are reduced to about 41, 39, and 18%, respectively). However, in perforated specimens with the Type-I arrangement, the values of normalized CHE and LHE and equivalent viscous damping ratio are lower than those in the perforated specimens with the Type-II arrangement (normalized CHE, LHE, and equivalent viscous damping ratio are reduced to about 28, 26, and 10%, respectively). This is because the infill plate of perforated specimens with Type-II arrangement has a larger surface area than that of the perforated specimens with the Type-I arrangement.

3.4. System strength

3.4.1. Different aspect ratios

Figure 12 shows the variations in the ultimate strength of SPSW with perforation ratios equal to 0.2 and 0.6 ($D/S = 0.2$, $D/S = 0.6$). It is evident that the ultimate strength ratios for the SPSW in the cases of perforation ratios of 0.3, 0.4, and 0.5 fall between the values of two cases shown in Figure 12, and they are omitted for brevity. The results reveal that the strength of the infill plates with a small perforation ratio is approximately equal for both arrays of perforations in the infill panel (Type-I and Type-II arrangements). However, the strengths of the infill plates in SPSWs with high perforation ratios ($D/S =$

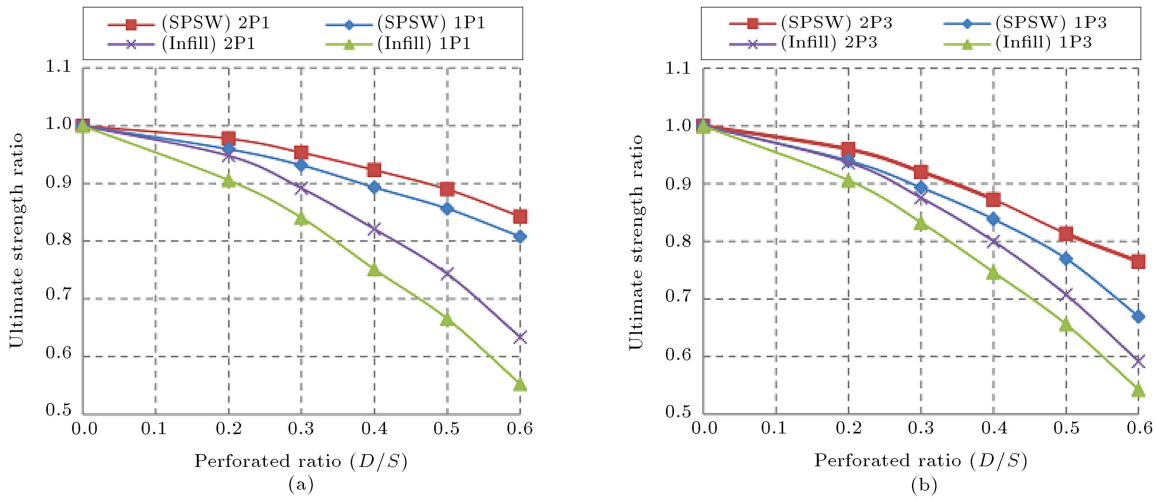

Figure 13. Variations of the ultimate strength ratios of frame, infill plate, and Steel Plate Shear Wall (SPSW) with different perforated ratios: (a) $L/H = 1$ and (b) $L/H = 3$.

0.6) are not equal. Based on a comparison between Figure 12(a) and 12(b), it can be concluded that by introducing perforations in the infill panels, the ultimate strength of the infill panels and, therefore, the ultimate strength of the specimens are reduced. Nevertheless, reduction in the ultimate strength of specimens with small perforation ratios is negligible (maximum reduced to 10%). Nevertheless, ultimate strength reduction for specimens with large perforation ratios is substantial (up to 46% reduction in case of $L/H = 3$ and $D/S = 0.6$ with the Type-I perforation arrangement). As a result, at aspect ratios lower than 2, the major reason for the reduction of specimen strength is the usage of perforated infill plates and this reduction trend decreases with increase in the aspect ratio of the specimen and becomes almost negligible at high aspect ratios.

3.4.2. Different perforation ratios

Figure 13 shows the variations in the ultimate strength ratios of the SPSW in two cases of aspect ratios 1 and 3 ($L/H = 1$, $L/H = 3$) for various perforation ratios. This figure confirms that in specimens with perforation ratios less than $D/S = 0.2$, the decrease in strength is negligible and it is almost linear. However, in specimens with perforation ratios ranging from $D/S = 0.2$ to $D/S = 0.6$, this rising trend in strength reduction increases (up to 46% reduction). This strength reduction occurred in the specimen with both perforation arrangements. However, in the infill plate with arrangement 1, the reduction is sharper. With a comparison between Figure 13(a) and (b), it can be concluded that by increasing the aspect ratios of the specimen from $L/H = 1$ to $L/H = 3$, the ultimate strength of the infill plate and specimen increased. However, the strength reduction for the specimens is greater than that for the infill plates (about 25% decreased in case of $L/H = 1$ and $D/S = 0.2$ with a Type-I perforation arrangement).

3.5. Interaction of frame-infill plate

Figures 13 and 14 show the contribution of the frame and infill plate to resisting the shear forces due to lateral load in 1- and 14-story specimens with an aspect ratio of $L/H = 2$ in different loading stages. The behavior of SPSWs with solid and perforated infill plates with perforation ratios of $D/S = 0.2$ and $D/S = 0.6$ is illustrated in Figures 14 and 15, respectively. The corresponding curves of other SPSWs with different perforation and bay ratios are similar and are not presented for brevity.

In general, the results show that in different stages of loading, the share of each frame and infill plate in resisting the lateral loads is different and one is larger than the other. In other words, in the initial stages of loading, the infill plates bear a large portion of shear forces. In the specimen with a solid infill plate (without perforations), the formation of the tension field reduces the role of the infill plate in withstanding shear forces and increases the share of the boundary frame. Increasing the displacement amplitude leads to the expansion of the tension field and the overall yield of the infill plate at a drift of about 1.35%. At this point, in all specimens with and without perforations, the role of the frame in bearing lateral loads has reached its maximum share.

In the perforated SPSWs, the loading contribution of the frame increases at lower drifts. For instance, in the case of single-story perforated SPSWs with perforation ratios of $D/S = 0.2$ and $D/S = 0.6$, the frame reaches its maximum contribution of load bearing at 1% and 1.15% drift ratios, respectively. With an increase in the number of the stories, the loading capacity of the infill plate decreases dramat-

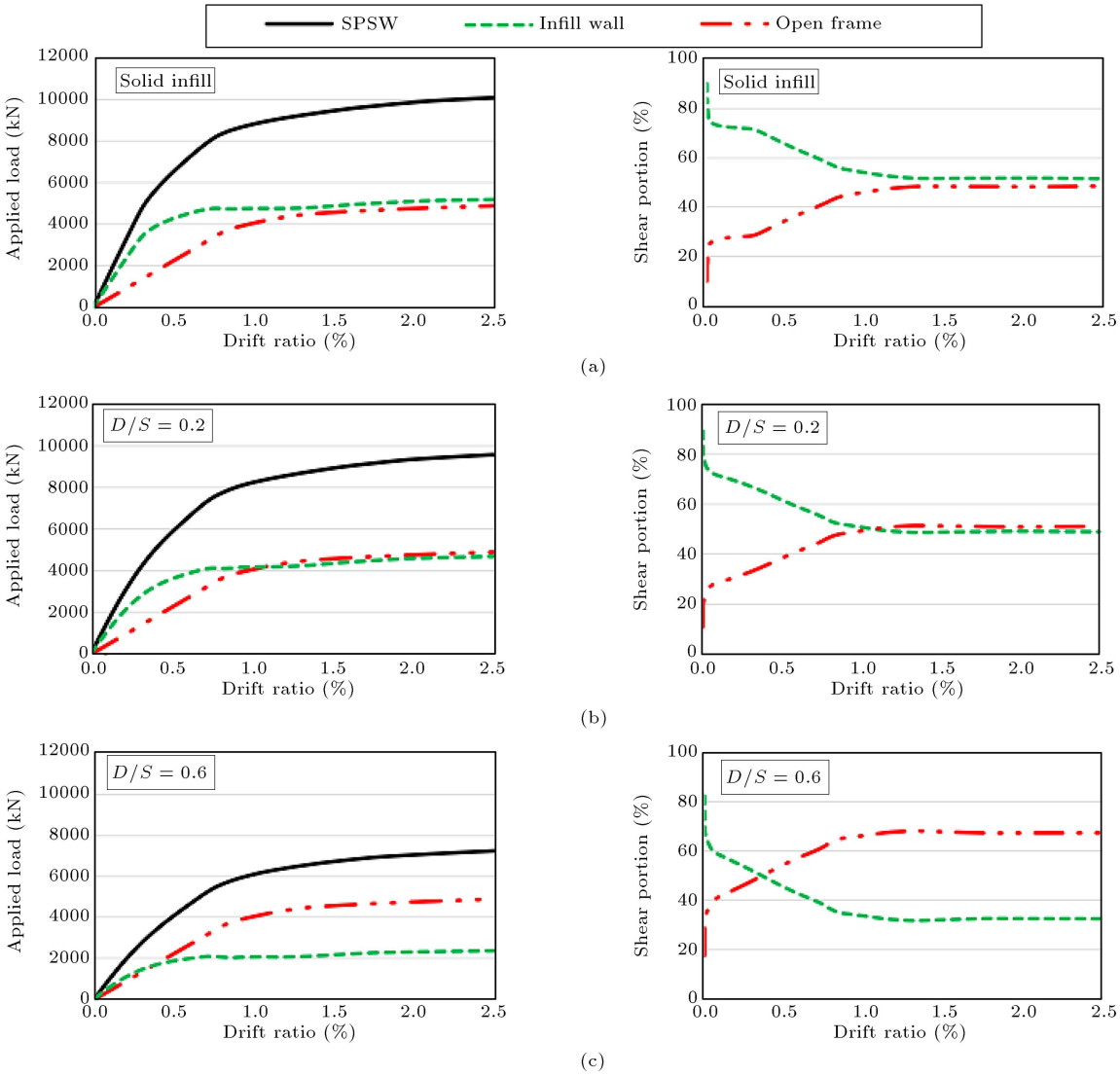

Figure 14. Shear capacity of typical single-story Steel Plate Shear Walls (SPSWs) ($L/H = 2$) and role of infill plates in bearing lateral loads with: (a) Solid infill plate, (b) perforated infill plate ($D/S = 0.2$), and (c) perforated infill plate ($D/S = 0.6$).

ically, even in the early stage of the loading. Thus, for all SPSWs with solid infill plates at a drift ratio of about 1.1%, the boundary frame reaches its maximum contribution to resisting the lateral loads. In high-rise perforated SPSWs with a conventional aspect ratio ($L/H < 2$), in the early stages of the loading, the maximum contribution to resisting the lateral loads belongs to the boundary frame. However, with the increase in the displacement amplitude (greater than 1.1% drift), in the perforated SPSWs, the infill plate has almost the same load-bearing ratio as compared to the SPSWs with solid infill plate (reduced role less than 4%).

The amount of shear forces tolerated by the infill plates decreases with increasing the frame height. This is due to the fact that in SPSWs design, the capacity of the frame and its boundary elements in resisting the lateral loads is conservatively ignored. In other words, it is assumed that the shear force of the entire structure is tolerated by the infill plates. These assumptions lead to the use of thicker infill plates and, thus, to larger cross-sections of VBEs (columns) and ultimately contributing to the larger shear capacity of the system. With increasing the number of stories and the shear forces, the infill plates on the lower stories are expected to become thicker, resulting in much larger cross-sections of VBEs. As a result, as shown in Figure 15, the share of shear force tolerated by the boundary frame in high-rise SPSWs is increased compared to the infill plates. It is important to note that the thickness of the infill plates and the sections of the boundary frame are assumed to be the same in both specimens with and without perforations as previously stated. These assumptions have led to the

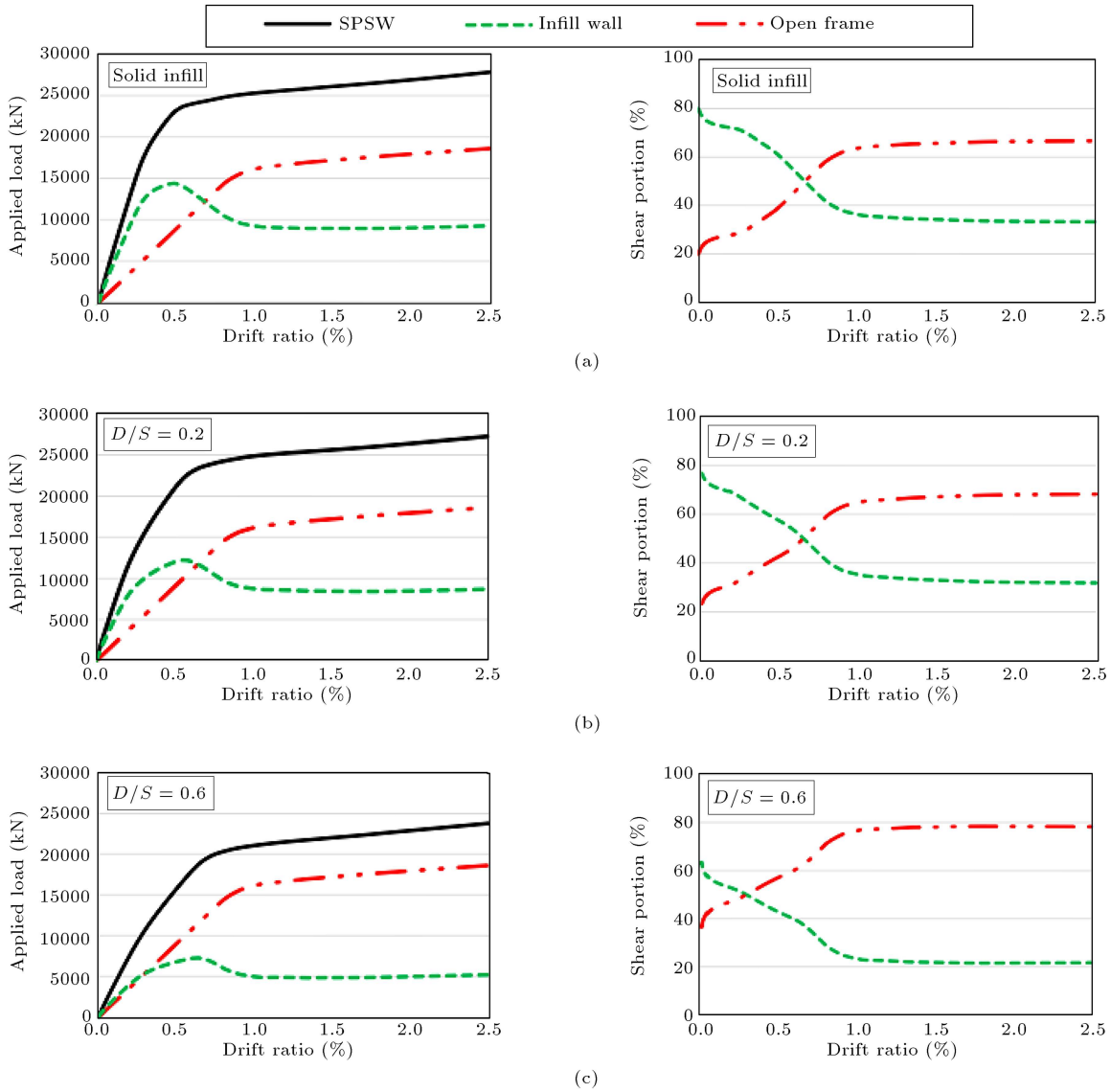

Figure 15. Shear capacity of typical 14-story Steel Plate Shear Walls (SPSWs) ($L/H = 2$) and role of infill plates in bearing lateral loads with: (a) Solid infill plate, (b) perforated infill plate ($D/S = 0.2$), and (c) perforated infill plate ($D/S = 0.6$).

insignificant role of the infill plates in resisting the shear force on the upper stories. With an increase in the number of stories, the possibility of the complete yield of the infill plates decreases across the height of the structure.

Accordingly, it can be concluded that by increasing the number of stories, especially on the upper stories, by reducing the share of the infill plate in resisting the lateral loads, the effect of introducing perforations on reduction of the loading capacity has decreased. For example, this loading capacity loss in infill plates for the specimens with a perforation ratio of $D/S = 0.6$ is about 5% compared to the specimen with solid infill plates (specimen 14S2). However, in low-rise SPSWs, the loss of the loading capacity is significant. For instance, the loading capacity loss of the infill plate in a specimen with a perforation ratio $D/S = 0.6$ is 17% in comparison with the specimen 1S2.

The results show that a decrease in the load-bearing capacity of the infill plate in single-story specimens due to the introduction of perforations is significant. Thus, in specimens with a large perforation ratio ($D/S = 0.6$) with a Type-I arrangement, the loading capacity of the infill plate and the total loading capacity of the sample compared to the control sample are reduced to 44 and 28%, respectively. In specimens with a large perforation ratio ($D/S = 0.6$) with the Type-I arrangement, the loading capacities of the infill plate and the specimen compared to the reference specimen are reduced to 44 and 28%, respectively.

As the number of stories increases, the amount of drop in the load-bearing ratio of the infill plate

Table 5. Values of ductility ratio and initial stiffness of Steel Plate Shear Wall (SPSW) specimens with different aspect ratios.

Number of stories, n	Aspect ratio, L/H	Model name	K (kN/mm)	μ
1	1	1S1	239.76	5.05
	1.5	1S1.5	302.4	5.15
	2	1S2	437.13	4.93
	2.5	1S2.5	559.25	4.79
	3	1S3	592.36	4.43
14	1	14S1	116.86	6.28
	2	14S2	128.76	8.05
	3	14S3	164.1	8.89

remains almost unchanged. The results show that with increasing the height of the structure, due to the reduction of the contribution of the infill plate to bearing lateral loads, the creation of perforations in the infill plate has a negligible effect on the load drop of the SPSW.

The decrease in the load capacity of the 14-story specimen with a perforation ratio of $D/S = 0.6$ compared to the same specimen with the solid infill plate is up to about 14% less than the decrease in the load-bearing capacity of the single-story specimen. As a result, utilization of perforated infill plates in high-rise specimens will not lead to a sharp drop in the loading capacity of the specimen due to the reduced role of infill plates in bearing lateral loads relative to the boundary frame. However, this indicates that the use of perforated infill plates in high-rise specimens compared to short specimens can increase the demand on columns and this should be considered in the design of columns. As a result, at conventional practical ratios ($L/H < 2$), by introducing perforations in the infill plates, the overall loading capacity loss ratio of the SPSW compared to the reference specimen decreases from 0.86 for the highest-rise specimen to 0.72 for the lowest-rise specimen.

3.6. Stiffness and ductility

As mentioned in Subsection 3.1, the SPSW with an unstiffened infill plate loses much of its stiffness in the early stages of loading due to early buckling. It is noteworthy that by creating perforations in the infill plates, the value of the initial stiffness of the system can experience a noticeable decline and lead to an effective reduction in the performance of the SPSW. In conventional SPSWs, buckling in the infill plate may occur through gravitational force and construction errors even before the application of lateral loads. Hence, an appropriate estimation of SPSW stiffness can be achieved by accounting for the initial buckling in the infill plates. To calculate the system stiffness, the reduction in stiffness due to early buckling in the infill plates has been considered.

Table 5 shows the stiffness (K) and ductility ratio (μ) of the reference SPSWs with solid, non-perforated infill plates. As shown earlier, the initial stiffness of SPSWs with solid infill plates generally decreases following an increase in the height of the structure and increases with increase in the bay width. The highest initial stiffness is for specimen 1S3 and the lowest initial stiffness belongs to specimen 14S1. Also, the ductility ratio of SPSWs with solid infill plates generally improves with increasing the bay width as well as the height of the structure. The ductility ratio of the shortest specimen with the lowest bay width is 5.05, and for the highest specimen with the largest bay width is 8.89. Table 6 shows stiffness (K') and ductility ratio (μ') of perforated SPSWs compared to the stiffness (K) and ductility ratio (μ) of the corresponding SPSWs with solid infill plates. Table 6 also shows the results for 1- and 14-story SPSWs with different aspect ratios varying between $L/H = 1$ and $L/H = 3$.

The nonlinear force-displacement relationship between the base shear and the roof displacement is replaced by an ideal bilinear diagram, according to Figure 16, to obtain equivalent stiffness, K_e and effective yield strength, V_y. Furthermore, the ideal force-displacement diagram is obtained according to the method proposed by FEMA-356 [53]. The maximum displacement ($\delta_{\max}$) has been considered as the displacement at the top of specimen at a displacement ratio of 2.5%. The yield displacement (δ_y) is obtained using the concept of equivalent plastic energy such that the bounded area by the ideal bilinear diagram is equivalent to the area enclosed by the practical push-over curve. All the required parameters in calculating ductility are shown in Figure 16.

The results reveal that due to the introduction

Table 6. Effects of introducing the opening on the values of the ductility ratio and initial stiffness of the Steel Plate Shear Wall (SPSW) specimens with different width/height ratios.

No. of stories	Pattern A					Pattern B				
	$D/S = 0.2$					$D/S = 0.2$				
				Ratio					Ratio	
	Aspect ratio, L/H	K' (kN/mm)	μ'	$\frac{K'}{K_{infill\ solid}}$	$\frac{\mu'}{\mu_{infill\ solid}}$	Aspect ratio, L/H	K' (kN/mm)	μ'	$\frac{K'}{K_{infill\ solid}}$	$\frac{\mu'}{\mu_{infill\ solid}}$
	1	198.84	3.1	0.83	0.61	1	206.11	3.2	0.86	0.63
	2	391.33	3.46	0.89	0.7	2	403.49	3.54	0.92	0.72
	3	419.94	3.19	0.71	0.72	3	434.56	3.3	0.73	0.74
	$D/S = 0.6$					$D/S = 0.6$				
1				Ratio					Ratio	
	Aspect ratio, L/H	K' (kN/mm)	μ'	$\frac{K'}{K_{infill\ solid}}$	$\frac{\mu'}{\mu_{infill\ solid}}$	Aspect ratio, L/H	K' (kN/mm)	μ'	$\frac{K'}{K_{infill\ solid}}$	$\frac{\mu'}{\mu_{infill\ solid}}$
	1	177.91	2.54	0.74	0.5	1	186.17	2.65	0.78	0.52
	2	291.57	3.03	0.67	0.61	2	308.43	3.14	0.71	0.64
	3	308.14	2.83	0.52	0.64	3	345.35	3.26	0.58	0.74
	$D/S = 0.2$					$D/S = 0.2$				
				Ratio					Ratio	
	Aspect ratio, L/H	K' (kN/mm)	μ'	$\frac{K'}{K_{infill\ solid}}$	$\frac{\mu'}{\mu_{infill\ solid}}$	Aspect ratio, L/H	K' (kN/mm)	μ'	$\frac{K'}{K_{infill\ solid}}$	$\frac{\mu'}{\mu_{infill\ solid}}$
	1	96.66	4.8	0.86	0.76	1	98.84	5.06	0.88	0.81
	2	115.27	5.65	0.90	0.7	2	118.84	5.78	0.92	0.72
	3	117.89	5.23	0.72	0.59	3	124.84	5.56	0.76	0.62
	$D/S = 0.6$					$D/S = 0.6$				
14				Ratio					Ratio	
	Aspect ratio, L/H	K' (kN/mm)	μ'	$\frac{K'}{K_{infill\ solid}}$	$\frac{\mu'}{\mu_{infill\ solid}}$	Aspect ratio, L/H	K' (kN/mm)	μ'	$\frac{K'}{K_{infill\ solid}}$	$\frac{\mu'}{\mu_{infill\ solid}}$
	1	73.64	4.2	0.66	0.67	1	76.62	4.33	0.68	0.69
	2	85.88	4.95	0.67	0.61	2	90.85	5.13	0.71	0.64
	3	91.4	4.55	0.57	0.51	3	100.7	4.98	0.61	0.56

of perforations in the infill plate, the stiffness of SPSW considerably decreases (up to %48). In general, the rate of decrease in the initial stiffness of the system increases as the aspect ratio and the system height increase. Therefore, the initial stiffness reduction is 17% for the single-story specimen with a perforation ratio of 0.2 (specimen 1P1S0.2) and 43% for the 14-story specimen with a perforation ratio of 0.6 (specimen 14P3S0.6). In addition, as it is illustrated in Table 6, the introduction of perforations in the infill plate significantly reduces the value of ductility ratio (up to 49%).

Plastic deformation of the infill plate is the most important source of SPSW ductility. Therefore, the introduction of perforation in infill plate will reduce the participation of the infill plate in the overall behavior of the system where the ductility decreases. Finally, the reduction rate of ductility ratio of the system increases upon increasing the aspect ratio and height of the specimen. This reduction in ductility ratio is 39% for the single-story specimen with a perforation ratio of 0.2 (specimen 1P1S0.2) and 49% for the 14-story specimen with a perforation ratio of 0.6 (specimen 14P3S0.6).

4. Conclusions

A number of 1- and 14-story Steel Plate Shear Walls

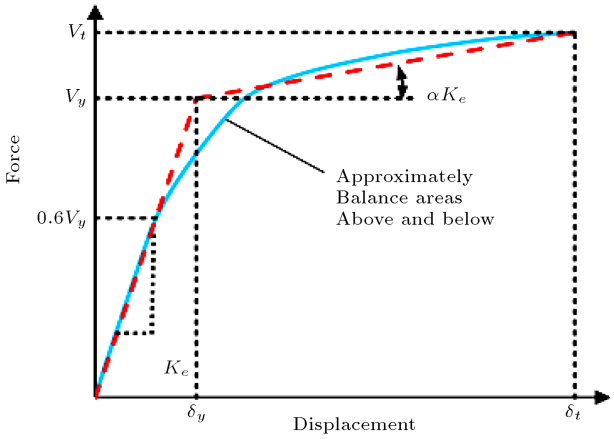

Figure 16. Idealized force-displacement curve.

(SPSWs) with solid and perforated infill panels with different perforation ratios and two different arrays were numerically analyzed, and the results were utilized to (a) ensure a better understanding of the behavior of SPSW with perforated infill plates at different aspect ratios, (b) determine the effects of perforations and different placement arrays of the perforations on the behavior of the system, (c) evaluate the change in the behavior of low- and high-rise structures by the introduction of perforations, and (d) study the effects caused by the introduction of perforations (variation in strength, ductility, and stiffness). The following conclusions can be drawn as follows:

- Comparison of the results showed that the presence of perforations had a significant effect on the ultimate strength, ductility ratio, and initial stiffness of the specimens (the ultimate strength, ductility ratio, and initial stiffness of the perforated SPSWs with the Type-I perforation pattern were reduced to 28, 29, and 33.5% compared to the reference specimen, respectively);
- The effect of introducing perforations on normalized Cumulative Hysteresis Energy (CHE) and Last cycle Hysteresis Energy (LHE) was considerable. In most perforated specimens, the normalized CHE and LHE values and the equivalent viscous damping ratio were significantly reduced compared to the reference specimen with a solid infill plate (normalized CHE and LHE values and the equivalent viscous damping ratio were reduced to about 41, 39, and 18%, respectively);
- The values of normalized CHE and LHE and equivalent viscous damping ratio in perforated specimens with Type-I arrangement were lower than in comparison with the perforated specimens with Type II arrangement (normalized CHE, LHE, and equivalent viscous damping ratio were reduced to about 28, 26, and 10%, respectively). This is because the infill plate of the perforated specimens with Type-II arrangement has a larger surface area than that of the perforated specimens with the Type-I arrangement;
- The strength of an infill plate with small perforation ratios was independent of perforation array placement and was approximately equal for both arrangements; yet, the strength of the infill plate with high perforation ratios was dependent upon the perforation array placement and was not equal. Thus, it was realized that the perforation ratio was not the only controlling factor in the strength and ductility of the shear wall specimens, and the strength and ductility of SPSW were also dependent upon the placement array of the perforations in the infill plate;
- The stiffness of SPSWs was considerably reduced by the introduction of perforations in the infill plate (up to %36 for the perforation ratio of 0.6). With increase in the aspect ratio of the system and perforation ratio (D/S), the stiffness of the system was reduced. However, the role of increase in D/S in the stiffness reduction for the system was greater than that with the aspect ratio incrimination;
- In all 1- to 14-story SPSWs without perforations, the boundary frame reached its maximum contribution in the form of bearing the shear forces at drift ratios of about 1.35% and 1.1%, respectively. However, in SPSWs with perforation, the boundary frame achieved its maximum contribution as in bearing the shear forces relatively at smaller drift ratios. Furthermore, following an increase in the perforation ratios, the corresponding value becomes smaller. The values of the smallest and largest opening widths were about 1% and 1.15%, respectively.

References

1. Sabelli, R. and Bruneau, M., *Design Guide 20: Steel Plate Shear Walls*, American Institute of Steel Construction, Chicago, IL, USA (2007).
2. Astaneh-Asl, A. "Seismic behavior and design of steel shear walls", *Structural Steel Educational Council Moraga*, CA (2001).
3. Habashi, H. and Alinia, M. "Characteristics of the wall-frame interaction in steel plate shear walls", *Journal of Constructional Steel Research*, **66**(2), pp. 150–158 (2010).
4. Alinia, M. and Shirazi, R.S. "On the design of stiffeners in steel plate shear walls", *Journal of Constructional Steel Research*, **65**(10–11), pp. 2069–2077 (2009).
5. Alinia, M., Habashi, H., and Khorram, A. "Nonlinearity in the postbuckling behaviour of thin steel shear panels", *Thin-Walled Structures*, **47**(4), pp. 412–420 (2009).

6. Hosseinzadeh, S. and Tehranizadeh, M. "Introduction of stiffened large rectangular openings in steel plate shear walls", *Journal of Constructional Steel Research*, **77**, pp. 180–192 (2012).
7. Thorburn, L.J., Montgomery, C.J., and Kulak, G.L. "Analysis of steel plate shear walls", Structural Engineering Report No. 107, Department of Civil Engineering, The University of Alberta, Edmonton (1983).
8. Timler, P.A. and Kulak, G.L. "Experimental study of steel plate shear walls", Structural Engineering Report No. 114, Department of Civil Engineering, The University of Alberta, Edmonton (1983).
9. Tromposch, E.W. and Kulak, G.L. "Cyclic and static behaviour of thin panel steel plate shear walls", Structural Engineering Report No. 145, Department of Civil Engineering, The University of Alberta, Edmonton (1987).
10. Caccese, V., Elgaaly, M., and Chen, R. "Experimental study of thin steel-plate shear walls under cyclic load", *Journal of Structural Engineering*, **119**(2), pp. 573–587 (1993).
11. Driver, R.G., Kulak, G.L., Kennedy, D.L., and Elwi, A.E. "Cyclic test of four-story steel plate shear wall", *Journal of Structural Engineering*, **124**(2), pp. 112–120 (1998).
12. Elgaaly, M. and Liu, Y. "Analysis of thin-steel-plate shear walls", *Journal of Structural Engineering*, **123**(11), pp. 1487–1496 (1997).
13. Rezai, M., *Seismic Behaviour of Steel Plate Shear Walls by Shake Table Testing*, University of British Columbia (1999).
14. Roberts, T.M. and Sabouri-Ghomi, S. "Hysteretic characteristics of unstiffened perforated steel plate shear panels", *Thin-Walled Structures*, **14**(2), pp. 139–151 (1992).
15. Sabouri-Ghomi, S., Mamazizi, S., and Alavi, M. "An investigation into linear and nonlinear behavior of stiffened steel plate shear panels with two openings", *Advances in Structural Engineering*, **18**(5), pp. 687–700 (2015).
16. Alavi, E. and Nateghi, F. "Experimental study on diagonally stiffened steel plate shear walls with central perforation", *Journal of Constructional Steel Research*, **89**, pp. 9–20 (2013).
17. Pellegrino, C., Maiorana, E., and Modena, C. "Linear and non-linear behaviour of steel plates with circular and rectangular holes under shear loading", *Thin-Walled Structures*, **47**(6–7), pp. 607–616 (2009).
18. Berman, J.W. and Bruneau, M. "Experimental investigation of light-gauge steel plate shear walls", *Journal of Structural Engineering*, **131**(2), pp. 259–267 (2005).
19. Vian, D., Bruneau, M., Tsai, K.C., and Lin, Y.C. "Special perforated steel plate shear walls with reduced beam section anchor beams. I: Experimental investigation", *Journal of Structural Engineering*, **135**(3), pp. 211–220 (2009).
20. Vian, D., Bruneau, M., and Purba, R. "Special perforated steel plate shear walls with reduced beam section anchor beams. II: Analysis and design recommendations", *Journal of Structural Engineering*, **135**(3), pp. 221–228 (2009).
21. Purba, R.H., *Design Recommendations for Perforated Steel Plate Shear Walls*, State University of New York at Buffalo (2006).
22. Emami, F. and Mofid, M. "On the improvement of steel plate shear wall behavior, using energy absorbent element", *Scientia Iranica*, **24**(1), pp. 11–18 (2017).
23. Akbari, H.A. and Mofid, M. "Parametric study and computation of seismic performance factors of braced shear panels", *Scientia Iranica*, **23**(2), pp. 460–474 (2016).
24. Paik, J.K. "Ultimate strength of perforated steel plates under edge shear loading", *Thin-Walled Structures*, **45**(3), pp. 301–306 (2007).
25. Valizadeh, H., Sheidaii, M., and Showkati, H. "Experimental investigation on cyclic behavior of perforated steel plate shear walls", *Journal of Constructional Steel Research*, **70**, pp. 308–316 (2012).
26. Bhowmick, A.K., Grondin, G.Y., and Driver, R.G. "Estimating fundamental periods of steel plate shear walls", *Engineering Structures*, **33**(6), pp. 1883–1893 (2011).
27. Moghimi, H. and Driver, R.G. "Column demands in steel plate shear walls with regular perforations using performance-based design methods", *Journal of Constructional Steel Research*, **103**, pp. 13–22 (2014).
28. Barkhordari, M., Asghar Hosseinzadeh, S., and Seddighi, M. "Behavior of steel plate shear walls with stiffened full-height rectangular openings", *Asian Journal of Civil Engineering*, **15**(5), pp. 741–759 (2014).
29. Afshari, M.J. and Gholhaki, M. "Shear strength degradation of steel plate shear walls with optional located opening", *Archives of Civil and Mechanical Engineering*, **18**(4), pp. 1547–1561 (2018).
30. Sabouri-Ghomi, S., Ahouri, E., Sajadi, R., and Alavi, M. "Stiffness and strength degradation of steel shear walls having an arbitrarily-located opening", *Journal of Constructional Steel Research*, **79**, pp. 91–100 (2012).
31. Bahrebar, M., Kabir, M.Z., Zirakian, T., Hajsadeghi, M., and Lim, J.B. "Structural performance assessment of trapezoidally-corrugated and centrally-perforated steel plate shear walls", *Journal of Constructional Steel Research*, **122**, pp. 584–594 (2016).
32. Deylami, A. and Daftari, H. "Non-linear. behavior of steel plate shear wall with large rectangular opening", In *Proceedings of the 12th World Conference on Earthquake Engineering*, pp. 1–7 (2000).
33. Farzampour, A., Laman, J.A., and Mofid, M. "Behavior prediction of corrugated steel plate shear walls with openings", *Journal of Constructional Steel Research*, **114**, pp. 258–268 (2015).

34. Saad-Eldeen, S., Garbatov, Y., and Soares, C.G. "Experimental failure assessment of high tensile stiffened plates with openings", *Engineering Structures*, **206**, p. 110121 (2020).

35. Shekastehband, B., Azaraxsh, A.A., Showkati, H., and Pavir, A. "Behavior of semi-supported steel shear walls: Experimental and numerical simulations", *Engineering Structures*, **135**, pp. 161–176 (2017).

36. Phillips, A.R. and Eatherton, M.R. "Computational study of elastic and inelastic ring shaped-steel plate shear wall behavior", *Engineering Structures*, **177**, pp. 655–667 (2018).

37. Mu, Z. and Yang, Y. "Experimental and numerical study on seismic behavior of obliquely stiffened steel plate shear walls with openings", *Thin-Walled Structures*, **146**, p. 106457 (2020).

38. Paslar, N., Farzampour, A., and Hatami, F. "Investigation of the infill plate boundary condition effects on the overall performance of the steel plate shear walls with circular openings", In *Structures*, **27**, pp. 824–836. Elsevier (2020).

39. Khan, N.A. and Srivastava, G. "Models for strength and stiffness of steel plate shear walls with openings", In *Structures*, **27**, pp. 2096–2113, Elsevier (2020).

40. Yekrangnia, M. and Asteris, P.G. "Multi-strut macromodel for masonry infilled frames with openings", *Journal of Building Engineering*, **32**, p. 101683 (2020).

41. Asteris, P.G., Cotsovos, D.M., Chrysostomou, C.Z., Mohebkhah, A., and Al-Chaar, G.K. "Mathematical micromodeling of infilled frames: state of the art", *Engineering Structures*, **56**, pp. 1905–1921 (2013).

42. Cavaleri, L., Zizzo, M., and Asteris, P.G. "Residual out-of-plane capacity of infills damaged by in-plane cyclic loads", *Engineering Structures*, **209**, p. 109957 (2020).

43. Lemonis, M.E., Asteris, P.G., Zitouniatis, D.G., and Ntasis, G.D. "Modeling of the lateral stiffness of masonry infilled steel moment-resisting frames", *Structural Engineering and Mechanics*, **70**(4), pp. 421–429 (2019).

44. Purba, R. and Bruneau, M. "Finite-element investigation and design recommendations for perforated steel plate shear walls", *Journal of Structural Engineering*, **135**(11), pp. 1367–1376 (2009).

45. Sabouri-Ghomi, S. and Sajjadi, S.R.A. "Experimental and theoretical studies of steel shear walls with and without stiffeners", *Journal of Constructional Steel Research*, **75**, pp. 152–159 (2012).

46. Roberts, T.M. and Ghomi, S.S. "Hysteretic characteristics of unstiffened plate shear panels", *Thin-Walled Structures*, **12**(2), pp. 145–162 (1991).

47. Sabouri-Ghomi, S. "Discussion of plastic analysis and design of steel plate shear walls" by Jeffrey Berman and Michel Bruneau, *Journal of Structural Engineering*, **131**(4), pp. 695–697 (2005).

48. Sabouri-Ghomi, S., Ventura, C.E., and Kharrazi, M.H. "Shear analysis and design of ductile steel plate walls", *Journal of Structural Engineering*, **131**(6), pp. 878–889 (2005).

49. Venture, SAC Joint, and Guidelines Development Committee. "Recommended seismic design criteria for new steel moment-frame buildings", **350**, Washington, DC, USA: Federal Emergency Management Agency (2000).

50. AISC, ANSI/AISC 358-05. "Prequalified connections for special and intermediate steel moment frames for seismic applications", Chicago (IL): American Institute of Steel Construction (2006).

51. SUT-DAM, version 4.0. User's Manual (2006).

52. Choi, I.-R. and Park, H.-G. "Steel plate shear walls with various infill plate designs", *Journal of Structural Engineering*, **135**(7), pp. 785–796 (2009).

53. Council, B.S.S. "Prestandard and commentary for the seismic rehabilitation of buildings", Report FEMA-356, Washington, DC (2000).

Biographies

Hadi Darvishi received the BSC degree in Civil Engineering from Sharif University of Technology, Tehran, Iran in 2009 and MSc degree in Structural Engineering from Sharif University of Technology, Tehran, Iran. He is a PhD Candidate in Structural and Earthquake Engineering at Center of Excellence in Structures and Earthquake Engineering, Civil Engineering Department, Sharif University of Technology, Tehran, Iran.

Masoud Mofid. His biography was not available at the time of publication.